

# Wafer-Level Etch Spatial Profiling for Process Monitoring from Time-Series with Time-LLM

Hyunwoo Kim\*, Munyoung Lee\*, Seung Hyub Jeon, Kyu Sung Lee  
Electronics and Telecommunications Research Institute  
Daejeon, Republic of Korea  
{kim.hw, munyounglee, shjeon00, kysung.lee}@etri.re.kr

**Abstract**—Understanding wafer-level spatial variations from in-situ process signals is essential for advanced plasma etching process monitoring. While most data-driven approaches focus on scalar indicators such as average etch rate, actual process quality is determined by complex two-dimensional spatial distributions across the wafer. This paper presents a spatial regression model that predicts wafer-level etch depth distributions directly from multichannel in-situ process time series. We propose a Time-LLM-based spatial regression model that extends LLM reprogramming from conventional time-series forecasting to wafer-level spatial estimation by redesigning the input embedding and output projection. Using the BOSCH plasma-etching dataset, we demonstrate stable performance under data-limited conditions, supporting the feasibility of LLM-based reprogramming for wafer-level spatial monitoring.

**Index Terms**—In-situ process monitoring, wafer-level spatial profiling, LLM reprogramming, time-series systems

## I. INTRODUCTION

Recent advances in deep learning and large language models (LLMs) have enabled data-driven real-time monitoring in semiconductor manufacturing. Specifically, methodologies such as virtual metrology (VM), fault detection and classification (FDC), and prognostics and health management (PHM) play a pivotal role in detecting yield excursions and process anomalies by leveraging in-situ process data [1]–[3]. Deposition and etching are critical processes that determine device geometry, and the in-situ time-series data collected during these steps serve as key indicators of process state. However, conventional in-situ signals primarily capture temporal dynamics and do not directly reflect intra-wafer spatial variations. As a result, predicting wafer-level spatial profiles from in-situ signals has become essential, as these profiles directly characterize uniformity, yield, and process drift.

Despite this importance, wafer-level spatial profile prediction remains limited. Prior studies largely focus on scalar indicators such as average etch rate or on coarse spatial descriptors using statistical or deep learning models [4]–[6], while end-to-end regression of wafer-level two-dimensional spatial fields from in-situ time-series data has been rarely explored. In addition, many existing approaches rely on proprietary and

small-scale datasets, which hampers systematic evaluation of generalization across diverse process conditions.

Recently, LLM-based time-series models pretrained on large-scale datasets have emerged as an alternative. Time-LLM [7] reprograms time-series inputs into the LLM token space via patch-based input transformations and conditions the model using domain knowledge and statistical priors through a Prompt-as-Prefix mechanism. By freezing the LLM backbone and optimizing only lightweight reprogramming modules, the framework achieves stable learning even in data-scarce regimes. However, Time-LLM is fundamentally designed for forecasting within the same numerical domain and cannot be directly applied to spatial regression tasks that map temporal in-situ signals to wafer-level two-dimensional profiles.

In this paper, we present a Time-LLM-based spatial regression framework for inferring wafer-level etch depth distributions directly from in-situ process parameter and optical emission spectroscopy (OES) time series. By systematically redesigning the input embedding and output projection layers, the proposed approach extends the Time-LLM paradigm beyond conventional temporal forecasting to support direct time-series-to-spatial regression. Experimental evaluation on the BOSCH plasma-etching dataset demonstrates accurate reconstruction of wafer-level spatial profiles and robust generalization under process drift, even in data-limited regimes. To the best of our knowledge, this work constitutes the first empirical study to perform wafer-level spatial profile prediction on the real-world BOSCH plasma-etching dataset, underscoring the potential of LLM-based reprogramming for advanced semiconductor process monitoring.

## II. RELATED WORK

### A. Virtual Metrology for Process Monitoring

With the increasing complexity of semiconductor manufacturing, virtual metrology has become an important technique for real-time process monitoring in yield management [1]. Prior studies utilized in-situ sensor data such as OES to predict scalar process outputs, including mean etch rate and film thickness [8]. Other studies extended these approaches to estimate etch profile parameters, such as etch depth and bowing critical dimension, by extracting plasma information variables [1], [9]. However, most VM approaches remain focused on point-wise predictions, limiting their ability to capture dense wafer-level spatial non-uniformity.

\* These authors contributed equally to this work.

This work was supported by the Technology Innovation Program (Development and Practice of an On-device AI Functionality and Performance Testing Framework based on NPU, RS-2025-02307650) funded by the Ministry of Trade Industry and Resources (MOTIR, Korea) and ETRI grant funded by the Korea government (26ZT1100, 26YT1100).

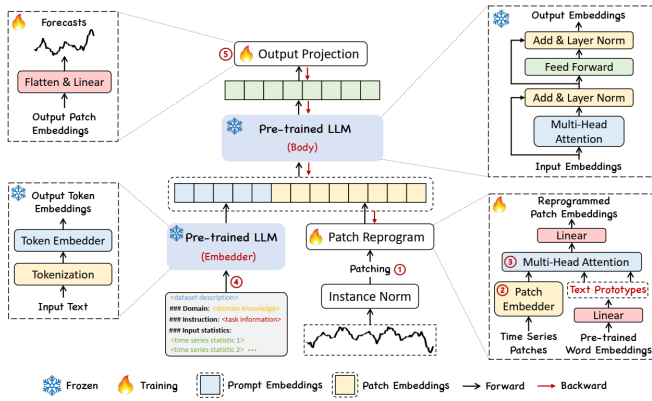


Fig. 1: Overall architecture of the Time-LLM framework, reproduced from [7].

### B. Data-Driven Spatial Etch Profiling

The modeling of wafer-level two-dimensional spatial profiles has evolved from classical statistical methods to modern data-driven deep learning approaches. Representative examples include Cascade RNNs (CRNNs) [4], hybrid Autoencoder-RBF models [5], and neural surrogate models trained on physics-based synthetic data [6]. Some studies further divided wafers into regions and predicted regional thickness uniformity from plasma signals [10]. Nevertheless, dense multi-point spatial regression remains challenging due to limited labeled data and increased model complexity.

### C. Time-Series-to-Spatial Regression via LLMs

Recent time-series research has demonstrated that frozen LLMs can serve as effective temporal feature extractors and enable few-shot forecasting [7], [11]–[14]. However, these approaches primarily address temporal forecasting within the same numerical domain, whereas wafer etch profile prediction requires mapping time-series signals to two-dimensional spatial outputs. In contrast, this work adapts LLM-based reprogramming to this cross-domain regression problem by restructuring the output layer for wafer-level spatial prediction.

## III. BACKGROUND

### A. Baseline model: Time-LLM

Time-LLM [7] is a forecasting framework that employs an LLM as a fixed backbone for time-series analysis. As shown in Fig. 1, the input time series is partitioned into patches and reprogrammed into the LLM embedding space via patch embedding and cross-attention, while data characteristics and task instructions are injected through a Prompt-as-Prefix (PaP) mechanism. The LLM processes the reprogrammed tokens together with the PaP to capture temporal patterns, and the resulting representations are mapped back to the numerical domain by an output projection layer to generate predictions. By freezing the LLM parameters and training only lightweight reprogramming and projection modules, Time-LLM enables stable learning in data-limited settings.

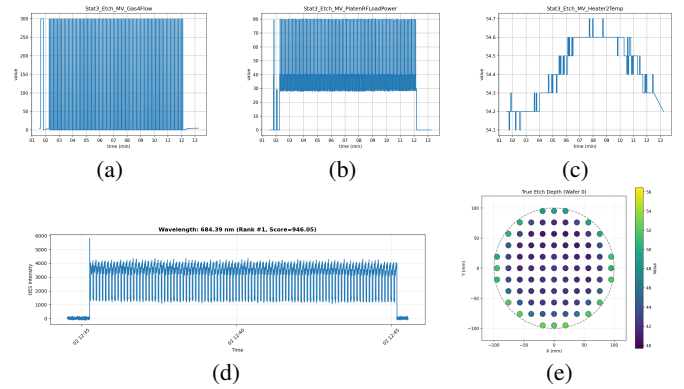


Fig. 2: Example in-situ and ex-situ data from the BOSCH DRIE dataset: (a) gas flow, (b) RF power, (c) heater temperature, (d) OES intensity, and (e) wafer-level etch depth profile.

### B. Target Domain: Silicon Etching Process

Plasma-based etching is a core semiconductor manufacturing process that achieves directional material removal through ion–radical interactions in the plasma, with process outcomes being highly sensitive to plasma chamber operating conditions. Process behavior is governed by chamber control parameters, including gas flow, RF power, chamber pressure, and temperature, which are collected as in-situ time-series data for monitoring and control. Since plasma states cannot be fully characterized by process parameters alone, OES is commonly employed to capture active species dynamics and plasma state variations in real time. Accordingly, multi-channel in-situ time series composed of process parameters and OES serve as a primary information source, and predicting wafer-level etch distributions and spatial non-uniformities from these signals is a key challenge for process monitoring and anomaly detection.

## IV. DATASET PREPARATION

### A. Dataset Overview

This study uses the BOSCH Deep Reactive Ion Etching (DRIE) dataset [15], collected from MEMS fabrication processes employing an  $\text{SF}_6/\text{C}_4\text{F}_8$ -based plasma etching scheme. Although acquired in a MEMS context, the dataset follows the same plasma-based etching mechanisms commonly used in semiconductor manufacturing. The dataset comprises fewer than 100 wafer-level etching runs, organized into multiple lots, each lot consisting of 10 wafers processed sequentially without chamber cleaning. This sequential processing within each lot induces cumulative chamber condition changes and process drift along the wafer order. For each run, in-situ process parameter and OES time series are provided together with wafer-level etch depth profiles measured at 89 locations. Representative examples are shown in Fig. 2. All runs were conducted under identical etch target conditions, allowing simultaneous observation of global wafer-to-wafer drift and intra-wafer spatial non-uniformity.

## B. Channel Selection

To ensure stable learning and generalization under a limited number of wafers, informative channels are selected from process parameter signals and OES data. Process parameter channels whose values exhibit negligible variance or extremely small standard deviation across the entire process duration and all wafers are removed, as they contribute little to prediction performance. OES channel selection is based on temporal intensity variability. Each wavelength is scored using the standard deviation and mean absolute temporal difference over the process cycle, with wafer-wise median aggregation applied for robustness. The top  $K$  wavelengths are selected, and non-maximum suppression (NMS) is applied along the wavelength axis to avoid redundant selection of adjacent bands.

## C. Dataset Conditioning

After feature and band selection, the active etching phase, during which plasma-assisted etching is performed, is identified from the in-situ time series using process parameter signals that directly reflect chamber operation, such as gas flow and RF power. The OES time series is then temporally aligned to this phase. The aligned process parameter and OES signals are resampled to match the fixed model input length and organized to ensure one-to-one correspondence at each time step. This procedure yields fixed-length, synchronized multi-channel in-situ inputs for each wafer, with the corresponding 89-point etch depth spatial profiles used as labels. After excluding wafers with missing data, a total of 88 wafers are used for evaluation.

## V. PROPOSED MODEL ARCHITECTURE

We propose a Time-LLM-based spatial regression model that predicts wafer-level etch depth distributions at 89 spatial locations from in-situ time-series data, including process parameters and OES signals. The overall architecture is illustrated in Fig. 3. The proposed framework follows the standard Time-LLM pipeline described in Section III-A, while introducing task-specific modifications to enable wafer-level spatial regression. In particular, the input embedding, prompt-as-prefix (PaP), output projection, and loss function are redesigned to map temporal in-situ signals directly to wafer-level spatial profiles, rather than to future time steps. The core design principle of Time-LLM—channel-independent time-series learning with a frozen LLM backbone—is preserved.

### A. Input Embedding

The input embedding stage transforms in-situ process time series into representations aligned with the LLM embedding space by partitioning the signals into patches and reprogramming each patch as a text prototype. The input consists of  $N_{pp}$  process parameter channels and  $N_{oes}$  OES bands selected through channel selection, resampled to  $N_T$  time steps over the entire etching process. Accordingly, each wafer is represented as a tensor of shape  $(N_c, N_T)$ , where  $N_c = N_{pp} + N_{oes}$ .

While the Time-LLM is designed for forecasting future values within the same numerical domain, this work uses the

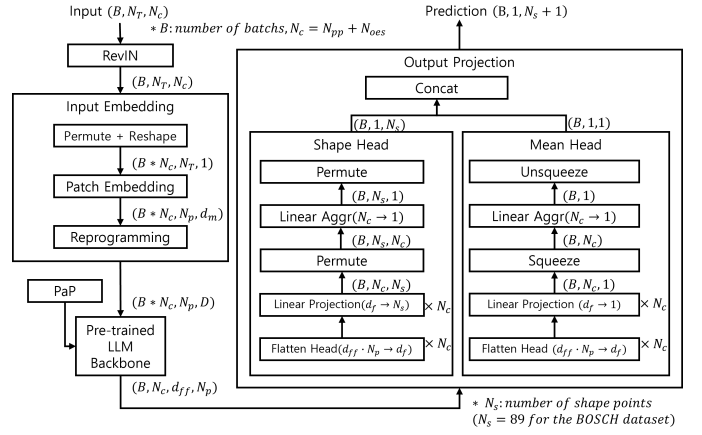


Fig. 3: Proposed model architecture.

entire process time series of a wafer as input and directly regresses a wafer-level spatial profile. To this end, the input embedding structure is reconfigured while preserving the core reprogramming concept of Time-LLM. Specifically, the embedding pipeline applies normalization followed by patch embedding and patch reprogramming, enabling the temporal process signals to be mapped to spatial regression outputs.

1) *Normalization*: Normalization is applied to the input time series to mitigate scale disparities across channels and to improve training stability. We adopt the RevIN-based normalization scheme used in Time-LLM; however, unlike forecasting tasks, denormalization is not applied at the output stage, reflecting the cross-domain nature of the regression task. Specifically, the inputs consist of process parameter and OES signals, whereas the outputs are wafer-level etch depths, for which scale recovery is unnecessary. The input signals are normalized on a per-wafer, per-channel basis using statistics computed over the entire etching process. These scale statistics are provided to the LLM through the Prompt-as-Prefix (PaP), allowing the model to retain scale-related information while operating on normalized inputs.

2) *Patch Embedding*: Patch embedding converts the normalized input time series into a sequence of local temporal representations by partitioning each channel into patches and projecting them into fixed-dimensional embeddings. In contrast to Time-LLM, which generates multiple training samples via sliding windows for forecasting, this work treats the entire process time series of a wafer as a single input of length  $N_T$ , which is used as the sequence length in the Time-LLM framework. The input sequence is then internally segmented into patches to form an LLM-compatible token sequence. Each process parameter and OES channel is divided into patches of length  $L_p$  with stride  $S$ , including boundary patches at the sequence ends, yielding  $N_p = \lfloor (N_T - L_p) / S \rfloor + 2$  patches per channel. Each patch is linearly projected into a  $d_m$ -dimensional embedding that summarizes local temporal patterns in the process signals.

$$\mathbf{X}^{(i)} \in \mathbb{R}^{N_p \times L_p} \xrightarrow{\text{Linear}} \hat{\mathbf{X}}^{(i)} \in \mathbb{R}^{N_p \times d_m}$$

3) *Patch Reprogramming*: Patch reprogramming maps the time-series tokens produced by patch embedding into word-token representations compatible with the LLM input space. In this work, we directly adopt the input reprogramming mechanism proposed in Time-LLM, as it has been shown to effectively align temporal patterns with the pretrained linguistic embedding space. Since the objective of this study is to extend Time-LLM from temporal forecasting to time-series-to-spatial regression, rather than to modify the reprogramming mechanism itself, the original structure is preserved. Specifically, the  $d_m$ -dimensional patch tokens are projected to the LLM backbone hidden dimension  $D$  using multi-head cross-attention followed by a linear transformation. With  $K$  attention heads, each head has dimensionality  $d = \lfloor d_m/K \rfloor$ :

$$\mathbf{X}^{(i)} \in \mathbb{R}^{N_p \times d_m} \xrightarrow{\text{Attention}} \{\hat{\mathbf{Z}}_k^{(i)} \in \mathbb{R}^{N_p \times d}\}_{k=1}^K$$

$$\text{Concat}(\hat{\mathbf{Z}}_1^{(i)}, \dots, \hat{\mathbf{Z}}_K^{(i)}) \xrightarrow{\text{Linear}} \hat{\mathbf{O}}^{(i)} \in \mathbb{R}^{N_p \times D}$$

The resulting sequence of  $N_p$  reprogrammed tokens is concatenated with the Prompt-as-Prefix (PaP) and fed into the LLM. Consistent with the channel-independent design of Time-LLM, each input channel is processed independently by the LLM during inference.

### B. Output Projection

The output projection stage maps the LLM output representations to wafer-level etch depth distributions at 89 spatial locations. To capture distinct sources of variation, the wafer-level etch depth is decomposed into a global mean component and a spatial shape component. The shape is defined as the spatial residual after removing the wafer-wise mean, representing morphological characteristics such as center-edge variation, ring patterns, and asymmetry. In contrast, the mean reflects the absolute etch level across the wafer and captures global drift induced by process condition changes or chamber aging. Given their different physical interpretations and variation mechanisms, these two components are predicted separately.

Compared with Time-LLM, which defines outputs in terms of prediction horizons and output channels for temporal forecasting, this work reformulates the output for time-series-to-spatial regression by setting the prediction horizon to one and redefining the output channels as 89 spatial shape values and a single mean value. Although the formulation corresponds to a single-step multi-channel output, it effectively performs regression over wafer-level spatial coordinates.

The output projection consists of three stages: a flatten layer, a linear projection layer, and a linear aggregation layer. While the flattening and per-channel projection follow the channel-independent design of Time-LLM, the projection and aggregation structures are redesigned to transform temporal representations into spatial regression outputs.

1) *Flatten Layer*: The flatten layer converts the LLM output representations into channel-wise one-dimensional vectors for subsequent projection, consistent with the baseline Time-LLM architecture. The LLM produces hidden representations of dimension  $D$  for each patch, from which the  $d_{ff}$ -dimensional

features excluding the prefix tokens are retained. Consequently, the output for each channel has shape  $\mathbb{R}^{N_p \times d_{ff}}$  and is flattened into a vector in  $\mathbb{R}^{d_f}$ , where  $d_f = N_p \cdot d_{ff}$ . This operation is applied to both the shape and mean heads.

2) *Linear Projection Layer*: The linear projection layer maps the channel-wise flattened vectors of dimension  $d_f$  to predictions defined over wafer spatial coordinates and a global mean. While the Time-LLM projects these representations to future prediction horizons for temporal forecasting, this work reformulates the projection to produce 89 spatial shape values and a single scalar mean value. For each input channel  $i$ , the shape head and mean head apply independent linear transformations to generate a channel-specific shape vector  $\hat{\mathbf{S}}^{(i)}$  and a mean estimate  $\hat{m}^{(i)}$ :

$$\hat{\mathbf{S}}_f^{(i)} \in \mathbb{R}^{d_f} \xrightarrow{\text{Linear}_s} \hat{\mathbf{S}}^{(i)} \in \mathbb{R}^{89}$$

$$\hat{\mathbf{M}}_f^{(i)} \in \mathbb{R}^{d_f} \xrightarrow{\text{Linear}_m} \hat{m}^{(i)} \in \mathbb{R}$$

This design enables the model to learn how the process information encoded in each input channel contributes independently to spatial distribution and global mean estimation.

3) *Linear Aggregation Layer*: The linear aggregation layer integrates the channel-wise shape and mean predictions to produce the final wafer-level outputs. Unlike the Time-LLM, where inputs and outputs reside in the same domain and channel-wise predictions can be used directly, the present task maps in-situ process time series to wafer-level spatial profiles. This cross-domain setting necessitates explicit aggregation of information across multiple input channels.

For the shape head, channel-specific predictions are linearly combined at each spatial point using shared aggregation weights across all locations. This design enforces a consistent interpretation of channel contributions over the wafer, while avoiding a location-dependent aggregation that would substantially increase the number of parameters and exacerbate overfitting under limited data:

$$\hat{s}_j^{raw} = \sum_{i=1}^{N_c} w_i^{shape} \hat{s}_j^{(i)}, \quad j = 1, \dots, 89$$

Since the aggregated shape prediction may contain a residual mean bias, the final shape output is obtained by removing the spatial average, yielding a zero-mean spatial profile:

$$\hat{s}_j = \hat{s}_j^{raw} - \mu_s, \quad \mu_s = \frac{1}{89} \sum_{j=1}^{89} \hat{s}_j^{raw}$$

The mean head aggregates channel-wise mean estimates through an independent linear combination to produce a single scalar mean value:

$$\hat{m} = \sum_{i=1}^{N_c} w_i^{mean} \hat{m}^{(i)}$$

As discussed earlier, no denormalization is applied at the output stage, and both predictions and ground-truth labels remain in their original scale. Normalizing the outputs would remove information about the absolute magnitude of spatial non-uniformity across wafers and obscure global drift induced by process condition changes or chamber degradation. Therefore, etch depth values are preserved in their physical scale throughout training and evaluation.

**Dataset description:** Semiconductor silicon etch process monitoring data. The dataset contains  $N_c$  sensor measurements sampled over  $N_T$  timesteps during a wafer fabrication etch process. Sensors include plasma parameters (RF power, gas flow, pressure, temperature) and optical emission spectroscopy (OES) intensities at various wavelengths. The task is to predict the spatial etch depth uniformity distribution across 89 measurement points on the wafer surface.

**Task instruction:** Predict the spatial etch profile at 89 wafer positions given  $N_c$  process sensor channels of  $N_T$  timesteps

Fig. 4: Prompt-as-Prefix (PaP) used in the Time-LLM configuration for wafer-level spatial etch profile prediction.

### C. Prompt-as-Prefix (PaP)

Prompt-as-Prefix (PaP) is a natural language prefix that conditions the LLM on how to interpret the subsequent time-series patch tokens. We adopt the PaP mechanism from Time-LLM and tailor its content to wafer-level spatial etch profile prediction in plasma etching processes. The PaP comprises a dataset description, a task instruction, and input statistics. The dataset description is customized to reflect etching process data and sensor modalities, while the task instruction is reformulated to predict an 89-point wafer-level spatial etch profile from in-situ process time series. The input statistics, which summarize temporal characteristics such as trends and lag information, follow the standard Time-LLM formulation. An example PaP is provided in Fig. 4.

### D. Loss Function

Since the wafer-level etch depth is predicted as an 89-point spatial shape and a global mean, the loss function accounts for errors in both components. The shape loss is defined as the mean squared error (MSE) over the 89 spatial points, with the mean loss computed analogously for the wafer-level mean. The overall objective is formulated as a weighted sum of the two terms, where the weighting factor  $\lambda$  controls their relative contributions:

$$\mathcal{L} = \|\hat{\mathbf{s}} - \mathbf{s}\|_2^2 + \lambda(\hat{m} - m)^2$$

Loss computation is performed directly on unnormalized predictions and ground-truth labels to preserve the absolute magnitude of spatial non-uniformity across wafers as well as global drift effects. To avoid degenerate solutions in which one branch dominates optimization,  $\lambda$  is treated as a fixed hyperparameter and selected via validation rather than being learned during training.

## VI. EXPERIMENTS

This section evaluates the proposed model in terms of shape MSE, mean MSE, and etch depth mean absolute error (MAE). We examine how input temporal resolution and patch configuration, the number of OES channels, and backbone LLM capacity affect wafer-level spatial profile prediction. Because direct wafer-level spatial profile prediction has been scarcely studied and existing approaches are largely restricted

TABLE I: 10-fold cross-validation errors (mean  $\pm$  std) for different patch length, stride, and sequence length.

| MSE (shape) |     |                 |                                   |                                   |                                   |
|-------------|-----|-----------------|-----------------------------------|-----------------------------------|-----------------------------------|
| $L_p$       | $S$ | $N_T=3000$      | $N_T=6000$                        | $N_T=9000$                        | $N_T=12000$                       |
| 32          | 16  | 0.42 $\pm$ 0.33 | 0.73 $\pm$ 0.41                   | 0.51 $\pm$ 0.21                   | <b>0.18 <math>\pm</math> 0.10</b> |
| 48          | 24  | 0.57 $\pm$ 0.35 | 0.37 $\pm$ 0.18                   | 0.59 $\pm$ 0.28                   | 0.44 $\pm$ 0.44                   |
| 64          | 32  | 0.65 $\pm$ 0.41 | 0.53 $\pm$ 0.40                   | 0.42 $\pm$ 0.12                   | 0.46 $\pm$ 0.20                   |
| MSE (mean)  |     |                 |                                   |                                   |                                   |
| $L_p$       | $S$ | $N_T=3000$      | $N_T=6000$                        | $N_T=9000$                        | $N_T=12000$                       |
| 32          | 16  | 6.26 $\pm$ 5.92 | 5.13 $\pm$ 4.66                   | 2.78 $\pm$ 2.67                   | 4.16 $\pm$ 3.67                   |
| 48          | 24  | 4.88 $\pm$ 5.30 | <b>2.28 <math>\pm</math> 2.00</b> | 7.54 $\pm$ 5.32                   | 3.99 $\pm$ 2.65                   |
| 64          | 32  | 4.10 $\pm$ 2.47 | 3.70 $\pm$ 3.29                   | 9.33 $\pm$ 4.41                   | 4.55 $\pm$ 7.46                   |
| MAE (etch)  |     |                 |                                   |                                   |                                   |
| $L_p$       | $S$ | $N_T=3000$      | $N_T=6000$                        | $N_T=9000$                        | $N_T=12000$                       |
| 32          | 16  | 1.88 $\pm$ 0.76 | 1.88 $\pm$ 0.89                   | <b>1.23 <math>\pm</math> 0.43</b> | 1.57 $\pm$ 0.82                   |
| 48          | 24  | 1.73 $\pm$ 0.92 | 1.25 $\pm$ 0.51                   | 2.23 $\pm$ 0.69                   | 1.61 $\pm$ 0.56                   |
| 64          | 32  | 1.64 $\pm$ 0.52 | 1.53 $\pm$ 0.71                   | 2.43 $\pm$ 0.55                   | 1.44 $\pm$ 0.91                   |

to scalar metrics, suitable baselines are limited. We therefore adopt a Global Mean Baseline that predicts a constant value equal to the training-set global mean for all wafers, to quantify the benefit of explicitly modeling spatial information. All experiments are conducted using lot-wise 10-fold cross-validation, reporting the mean and standard deviation across folds, and are performed on two NVIDIA A100 GPUs (80GB).

### A. Input Temporal Resolution Sensitivity Analysis

We evaluate the effect of input temporal resolution ( $N_T$ ) and patch configuration ( $L_p, S$ ) on wafer-level spatial profile prediction. Experiments use GPT2-small (6 layers) for computational efficiency, with input channels fixed to  $N_c=73$  ( $N_{pp}=25, N_{oes}=48$ ). The temporal resolution  $N_T$  is varied by adjusting the sampling rate over the same active etching phase, subject to the backbone context-length constraint. As summarized in Table I, spatial shape MSE consistently decreases with increasing  $N_T$ , reaching its minimum at  $L_p=32, S=16$ , and  $N_T=12000$ , which indicates that finer temporal resolution improves spatial pattern recovery. In contrast, mean MSE shows no monotonic trend with  $N_T$  and varies substantially across configurations, reflecting the stronger influence of global factors such as process drift. The final etch depth MAE generally improves under configurations that yield lower shape error, highlighting the critical role of accurate spatial reconstruction. Patch configuration also affects performance: overly large patches obscure local temporal patterns, whereas excessively small patches are limited by context length and training stability. Overall, intermediate ( $L_p, S$ ) settings offer the best balance between accuracy and robustness.

### B. Input Channel Sensitivity Analysis

This experiment examines the effect of the number of OES input channels on wafer-level etch spatial profile prediction. Using GPT2-small (6 layers) as the backbone, we fix the patch and temporal settings to  $L_p=48, S=24$ , and  $N_T=6000$ , and

TABLE II: 10-fold cross-validation errors (mean  $\pm$  std) for different numbers of OES channels.

| $N_{\text{o es}}$ | $N_c$ | MSE (shape)                       | MSE (mean)                        | MAE (etch)                        |
|-------------------|-------|-----------------------------------|-----------------------------------|-----------------------------------|
| 12                | 37    | 1.11 $\pm$ 0.98                   | 2.60 $\pm$ 3.76                   | 1.31 $\pm$ 0.77                   |
| 24                | 49    | 0.42 $\pm$ 0.22                   | 3.80 $\pm$ 3.62                   | 1.52 $\pm$ 0.73                   |
| 48                | 73    | 0.37 $\pm$ 0.18                   | <b>2.28 <math>\pm</math> 2.00</b> | <b>1.25 <math>\pm</math> 0.51</b> |
| 72                | 97    | <b>0.23 <math>\pm</math> 0.08</b> | 2.69 $\pm$ 2.31                   | 1.36 $\pm$ 0.56                   |

TABLE III: 10-fold cross-validation errors (mean  $\pm$  std) for different model backbones and input channel configurations.

| Backbone                    | L  | Ch | MSE (shape)                       | MSE (mean)                        | MAE (etch)                        |
|-----------------------------|----|----|-----------------------------------|-----------------------------------|-----------------------------------|
| LLaMA                       | 12 | 49 | <b>0.19 <math>\pm</math> 0.07</b> | 3.20 $\pm$ 2.58                   | 1.42 $\pm$ 0.56                   |
| LLaMA                       | 6  | 49 | 0.22 $\pm$ 0.07                   | <b>2.89 <math>\pm</math> 2.14</b> | <b>1.41 <math>\pm</math> 0.49</b> |
| LLaMA                       | 6  | 73 | 0.26 $\pm$ 0.14                   | 3.23 $\pm$ 2.87                   | 1.50 $\pm$ 0.62                   |
| GPT2                        | 12 | 73 | 0.33 $\pm$ 0.13                   | 3.59 $\pm$ 1.92                   | 1.53 $\pm$ 0.43                   |
| GPT2                        | 6  | 73 | 0.53 $\pm$ 0.40                   | 3.70 $\pm$ 3.29                   | 1.53 $\pm$ 0.71                   |
| <i>Global Mean Baseline</i> |    |    | 12.91 $\pm$ 0.37                  | 0.16 $\pm$ 0.07                   | 2.97 $\pm$ 0.04                   |

progressively increase the number of OES channels  $N_{\text{o es}}$  by adjusting the NMS window in the channel selection stage. As reported in Table II, spatial shape prediction accuracy improves overall as  $N_{\text{o es}}$  increases, achieving the lowest shape MSE at  $N_{\text{o es}}=72$ . In contrast, mean prediction accuracy and the final etch depth MAE are optimized at  $N_{\text{o es}}=48$  and exhibit a slight degradation when the channel count is further increased to 72. These results suggest that while a larger set of wavelengths enhances reconstruction of spatial distribution patterns, excessive spectral information may introduce redundancy or noise for predicting global scalar quantities such as the wafer-level mean.

### C. Backbone and Model Capacity Analysis

This experiment evaluates the effects of backbone LLM choice, model depth, and input channel dimensionality on wafer-level etch spatial profile prediction. Owing to GPU memory constraints, the context length is limited to approximately 300 tokens; accordingly, the input configuration is fixed to  $N_T=6000$  with  $L_p=64$  and  $S=32$  to focus on backbone and capacity effects. As reported in Table III, LLaMA-based models consistently outperform GPT2 across shape MSE, mean MSE, and etch depth MAE, highlighting the critical role of pretrained backbone representations in spatial profile prediction. Increasing model depth improves shape prediction, with LLaMA 12-layer models achieving lower shape error, whereas mean prediction and MAE are more stable under the LLaMA 6-layer setting, indicating that spatial structure and global magnitude rely on different representational capacities. Increasing the number of input channels from 49 to 73 does not lead to further performance gains under these settings. Although the Global Mean Baseline yields low mean MSE, it does not model spatial variation. In contrast, the proposed LLaMA-based model explicitly predicts spatial profiles and achieves competitive etch depth MAE despite solving a more demanding task, demonstrating its ability to recover wafer-

level spatial information from in-situ process time series beyond simple averaging.

## VII. CONCLUSION

In this paper, we proposed a Time-LLM-based spatial regression model for predicting wafer-level etch depth distributions at 89 spatial locations directly from in-situ process parameter and OES time-series data. By decomposing the prediction into global mean and spatial shape components, the proposed model jointly captures process-level drift and intra-wafer spatial non-uniformity in a structured and interpretable manner. To the best of our knowledge, this study represents one of the first empirical investigations that leverage the BOSCH plasma-etching dataset for wafer-level spatial profile prediction using an LLM-based reprogramming framework. Experimental results demonstrate that the proposed model can stably recover two-dimensional wafer-level etch patterns under data-limited conditions, while achieving competitive accuracy in wafer-level prediction. These findings provide quantitative evidence that LLM-based reprogramming constitutes a viable and effective approach for modeling wafer-level spatial characteristics in plasma etching processes, extending beyond conventional scalar virtual metrology paradigms.

## REFERENCES

- [1] V. Maitra *et al.*, "Virtual metrology in semiconductor manufacturing: Current status and future prospects," *Expert Systems with Applications*, 2024.
- [2] S. H. Kim *et al.*, "Machine learning-based process-level fault detection and part-level fault classification in semiconductor etch equipment," *IEEE Transactions on Semiconductor Manufacturing*, 2022.
- [3] A. J. *et al.*, "Predicting time-to-failure of plasma etching equipment using machine learning," in *International Conference on Prognostics and Health Management (ICPHM)*, 2019.
- [4] Z. Yao *et al.*, "Etching process prediction based on cascade recurrent neural network," *Engineering Applications of Artificial Intelligence*, 2025.
- [5] A. P. Pamarty *et al.*, "Data-driven surrogate model for etch rate profiles using sensor data from a reactive ion etcher," 2024, arXiv:2409.12925.
- [6] P. R. Kota, "Real-time plasma etch rate optimization using machine learning-based neural network surrogate models," 2025, techRxiv preprint.
- [7] M. Jin *et al.*, "Time-llm: Time series forecasting by reprogramming large language models," in *International Conference on Learning Representations (ICLR)*, 2024.
- [8] J. E. Choi and S. J. Hong, "Machine learning-based virtual metrology on film thickness in amorphous carbon layer deposition process," *Measurement: Sensors*, 2021.
- [9] J.-W. Kwon *et al.*, "Development of virtual metrology using plasma information variables to predict si etch profile processed by sf6/o2/ar capacitively coupled plasma," *Materials*, 2021.
- [10] H. Lee, "Development of pi-vm for etch control in wafer edge region," Master's thesis, Seoul National University, 2024.
- [11] T. Zhou *et al.*, "One fits all: Power general time series analysis by pretrained lm," in *Advances in Neural Information Processing Systems (NeurIPS)*, 2023.
- [12] C. Chang *et al.*, "Llm4ts: Aligning pre-trained llms as data-efficient time-series forecasters," *ACM Trans. Intell. Syst. Technol.*, 2025.
- [13] N. Gruver *et al.*, "Large language models are zero-shot time series forecasters," in *Advances in Neural Information Processing Systems (NeurIPS)*, 2023.
- [14] A. F. Ansari *et al.*, "Chronos: Learning the language of time series," *Transactions on Machine Learning Research*, 2024.
- [15] M. A. Sayyed *et al.*, "A multi-model dataset for bosch plasma-etching: Optical emission spectra, process parameters, and wafer measurements for data-driven plasma modeling," 2025.